Cell Biology
Stem Cells and Regenerative Medicine

The bile acid receptor TGR5 regulates the hematopoietic support capacity of the bone marrow niche

Alejandro Alonso-Calleja, Alessia Perino, Frédérica Schyrr, Silvia Ferreira Lopes, Vasiliki Delitsikou, Antoine Jalil, Ulrike Kettenberger, Dominique P. Pioletti, Kristina Schoonjans, Olaia Naveiras

Laboratory of Regenerative Hematopoiesis, Department of Biomedical Sciences, University of Lausanne, Switzerland • Laboratory of Metabolic Signaling, Institute of Bioengineering, Ecole Polytechnique Fédérale de Lausanne, Lausanne, Switzerland • Laboratory of Biomechanical Orthopedics, Ecole Polytechnique Fédérale de Lausanne, Lausanne, Switzerland • Hematology Service, Departments of Oncology and Laboratory Medicine, Lausanne University Hospital (CHUV) and University of Lausanne (UNIL), Lausanne, Switzerland

Reviewed Preprint

Published from the original preprint after peer review and assessment by eLife.

About eLife's process

Reviewed preprint version 1
January 24, 2024 (this version)

Posted to preprint server
November 23, 2023

Sent for peer review
November 21, 2023

Abstract

The gut is an emerging regulator of bone marrow (BM) hematopoiesis and several signaling molecules are involved in this communication. Among them, bile acids (BAs), originally classified as lipid solubilizers, have emerged as powerful signaling molecules that act as a relay between the digestive system, the microbiota and the rest of the body. The signaling function of BAs relies on specific receptors, including Takeda-G-protein-receptor-5 (TGR5). TGR5 has potent regulatory effects in immune cells, but its effect on the BM as a primary immune organ remains unknown. Here, we investigated the BM of young mice and observed a significant reduction in bone marrow adipose tissue (BMAT) upon loss of TGR5, accompanied by an enrichment in BM adipocyte progenitors which translated into enhanced hematopoietic recovery upon transplantation. These findings open the possibility of modulating stromal hematopoietic support by acting on TGR5 signaling.

Summary

This work shows that TGR5 loss-of-function reduces regulated bone marrow adipose tissue and accelerates recovery upon bone marrow transplantation. These data highlight TGR5 as key player of the bone marrow microenvironment.

eLife assessment

This study investigates the role of the bile acid receptor TGR5 in adult hematopoiesis of the mouse model. The findings are potentially **useful** because the loss of TGR5 leads to dysregulation of bone marrow adipose tissue (BMAT) that has emerging regulatory functions. However, the study is still **incomplete** because the mechanism of TGR5 is not clear, the stromal cells expressing TGR5 have not been well defined, and there is not strong evidence for the role of TGR5 in recovery from transplant stress.

Introduction

The bone, long considered a merely structural organ, is now seen as a highly dynamic tissue in which various processes, including hematopoiesis, bone remodeling, immunity and metabolism are tightly regulated[1,2]. These processes rely on specialized microenvironments, termed niches, that play a critical role in cell fate regulation[3], with the bone marrow adipose tissue (BMAT) being an emerging niche component[4–8]. The bone marrow (BM) niche regulates hematopoietic stem and progenitor cell (HSPC) quiescence, self-renewal and commitment towards differentiated cells thanks to a combination of soluble factors and cell-cell interactions[1,3,9,10]. Osteoblasts, adipocytes and endothelial cells form the BM niche along with a wide range of BM stromal cells (BMSCs) [1,11]. While the involvement of these specific cell types in the regulation of hematopoiesis is generally accepted, the extent of their action is controversial, especially for cells that form part of the adipocytic lineage. Mature BM adipocytes were first described to have a predominantly negative effect on hematopoietic recovery post-myeloablation[4,12,13]. Subsequent studies showing a positive effect of the BM adipocyte lineage on hematopoietic recovery called these results into question[5,14,15]. Recent work has uncovered a more nuanced role of non-lipidated BM adipogenic precursors in the control of bone homeostasis[6,7] and favoring hematopoietic recovery upon irradiation[8,16]. As for other adipose depots, the BMAT is plastic and can be remodeled upon injury and dietary or pharmacological stimulation[13,17–21].

Bone and BM homeostasis is influenced by extramedullary mechanisms, including the incompletely understood gut-BM cross-talk[22–25]. Communication between the gut and distant organs can be mediated by different signaling molecules, including bile acids (BAs), metabolites derived from the liver and modified by the gut microbiome[26]. BAs are signaling molecules that modulate whole-body metabolism[27–29] through activation of specific receptors that include the G protein-coupled receptor Takeda-G-protein-receptor-5 (TGR5)[30]. BA-TGR5 signaling has been studied in a multitude of organs[28,29], and profoundly affects adipose tissue physiology through several mechanisms, ranging from beiging[31,32] and suppression of chronic inflammation in resident macrophages of the white adipose tissue (WAT)[33], to stimulation of fat oxidation in brown adipose tissue (BAT)[34–36]. In addition, TGR5 expression was observed in human BMSC-derived adipocytes[32], but the effect of TGR5 on BMAT and thus on BM function is unknown. Previous reports have shown that BAs impact fetal and adult hematopoiesis acting as chemical chaperones[37–39] and, more recently, through direct interaction with myeloid blood cell precursors via the vitamin D receptor[40]. However, the effects at the level of TGR5, a BA-specific and potentially druggable receptor, remain to be unraveled.

Here, we report that TGR5 regulates the BM adipocytic lineage and hematopoietic recovery upon transplantation. We show that the loss of TGR5 markedly decreases BMAT in chow- and high-fat-diet (CD and HFD, respectively) conditions. Concomitantly, we observe an increase of

immunophenotypically-defined adipocyte-progenitor cells (APCs)[13] and a hastened hematopoietic recovery upon BM transplantation that is not dependent on the hematopoietic cells transplanted but on the genotype of the recipient.

Results

We first aimed to define the presence of TGR5 in primitive and differentiated hematopoietic populations. For this, we took advantage of a GFP reporter mouse model driven by the *Tgr5* promoter (TGR5:GFP)[41]. Flow cytometry analysis of hematopoietic populations showed consistent GFP signal throughout the main hematopoietic stem and progenitor (HSPC) populations in the adult mouse BM (**Fig. 1A**). We observed significant levels of GFP positivity in the lineage negative (Lin^-), c-Kit^+, $Sca1^+$ cells (LKS), a population highly enriched in murine hematopoietic stem and multipotent progenitor cells (**Fig. 1B**). We detected similar frequencies of GFP^+ cells in restricted myeloid progenitors with no marked differences in the percentage of GFP^+ cells between the different immunophenotypically defined subpopulations (granulocyte-monocyte progenitors (GMP), common myeloid progenitors (CMP) and megakaryocyte-erythrocyte progenitors (MEP) (**Fig. 1C**). GFP expression was further detected by immunohistochemistry in the BM (**Fig. 1D**), spleen (**Fig. S1A**) and thymus (**Fig. S1B**), confirming the expression of TGR5 in different immune organs. Flow cytometry analysis of fully differentiated hematopoietic populations in peripheral blood (**Fig. S1C**) showed that TGR5 is mostly expressed in cells of the myeloid lineage with lower expression in lymphocytes (**Fig. S1D**). Taken together, these findings indicate that TGR5 is present in primitive and differentiated hematopoietic cells.

We next aimed at defining the impact of a loss-of-function of TGR5 in hematopoiesis. Flow cytometry analysis of the BM of young germline TGR5 knock-out ($Tgr5^{-/-}$) mice showed no marked alterations in the percentage (**Fig. 2A**) or absolute number (**Fig. 2B**) of HSPC populations compared to their controls ($Tgr5^{+/+}$). Functionally, we could not detect differences in hematopoietic colony-forming unit (CFU) potential, and thus functional blood cell progenitors, between $Tgr5^{-/-}$ mice and their $Tgr5^{+/+}$ counterparts (**Fig. S2A**). However, we observed an increase in the total number of $CD45^+$ cells per hindlimb collected from $Tgr5^{-/-}$ animals (**Fig. 2C**) that did not lead to an increase in CFUs per hindlimb (**Fig. S2B**). Complete blood counts (CBC) of peripheral blood showed a modest increase in the number of red blood cells and a decrease in eosinophils, but no change in other white blood cells or platelets in $Tgr5^{-/-}$ mice (**Fig. 2, D-H**). Taken together, these results indicate that TGR5 is non-essential for steady-state hematopoiesis in young adult male mice.

In the next step, we aimed at defining the hematopoietic cell-autonomous effects of a germline deletion of TGR5 upon hematopoietic stress. For this, we examined the repopulating capacity of $Tgr5^{-/-}$ and $Tgr5^{+/+}$ BM cells when co-transplanted with competitor CD45.1.2 BM into a lethally irradiated wild-type recipient (CD45.1) (**Fig. 2I**). We found that, upon primary transplantation, $Tgr5^{-/-}$ donor cells blunt short-term repopulating capacity, but do not affect long-term repopulation (**Fig. 2J**) nor short-term repopulating capacity in the secondary or tertiary transplant (**Fig. S2C**). Taken together, these findings indicate that $Tgr5^{-/-}$ BM cells exhibit a transient deficit in short-term repopulating capacity that is corrected over serial transplantation in wild-type recipients, with no detectable long-term impairment of hematopoietic stem cell function.

Based on our findings that functional hematopoietic progenitors are quantitatively conserved at homeostasis and that the cell-autonomous effects disappear on serial transplantation (i.e., exposure to a wild-type BM niche), we hypothesized that an altered BM microenvironment in $Tgr5^{-/-}$ animals may account for this phenotype. In agreement with the literature[42], we found that young adult $Tgr5^{-/-}$ male mice display a decrease in bone volume fraction (BV/TV) and a decrease in trabecular number (Tb.N) with no changes in trabecular thickness (Tb.Th) or separation (Tb.Sp) at the distal femur (**Fig. 3**, A and B). In addition, no alterations in cortical

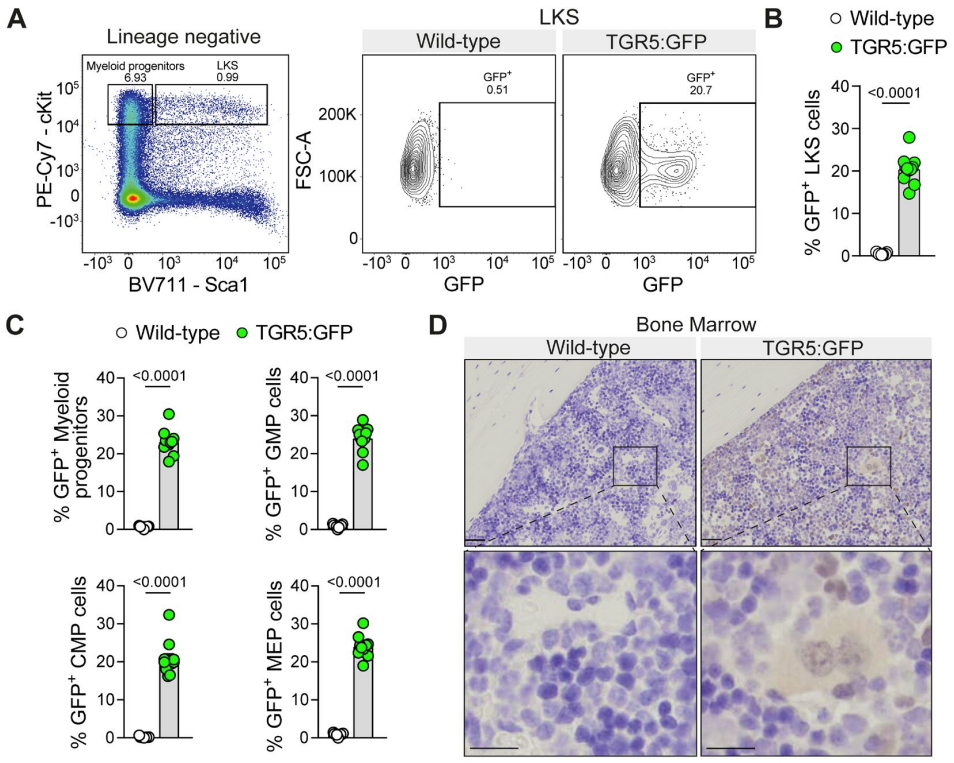

Figure 1.

TGR5 is expressed in BM hematopoietic stem and progenitor cells (HSPCs) and differentiated myeloid populations

A, representative flow cytometry gating strategy used to identify HSPCs and GFP positivity in TGR5:GFP mice and their wild-type controls. **B**, frequencies of GFP^+ cells in the $lineage^-cKit^+Sca1^+$ (LKS) population in the BM of 8-12-week-old male TGR5:GFP mice and their controls (n=9 for wild-type control mice, n=11 for TGR5:GFP mice). **C**, frequencies of GFP^+ cells in myeloid progenitors, common myeloid progenitors (CMP), granulocyte-monocyte progenitors (GMP) and megakaryocyte-erythrocyte progenitors (MEP) in the BM of 8-12-week-old male TGR5:GFP mice and their wild-type controls (n=9 for wild-type control mice, n=11 for TGR5:GFP mice). **D,** immunodetection of GFP^+ cells by DAB immunohistochemistry in BM of 8-12-week-old male TGR5:GFP mice (n=2 for wild-type control mice, n=3 for TGR5:GFP mice). Scale bar: 50 μm in low magnification images, 20 μm in the corresponding digitally zoomed images. Results represent the mean ± s.e.m., n represents biologically independent replicates. Two-tailed Student's t-test (**B** and **C**) was used for statistical analysis. P values (exact value) are indicated.

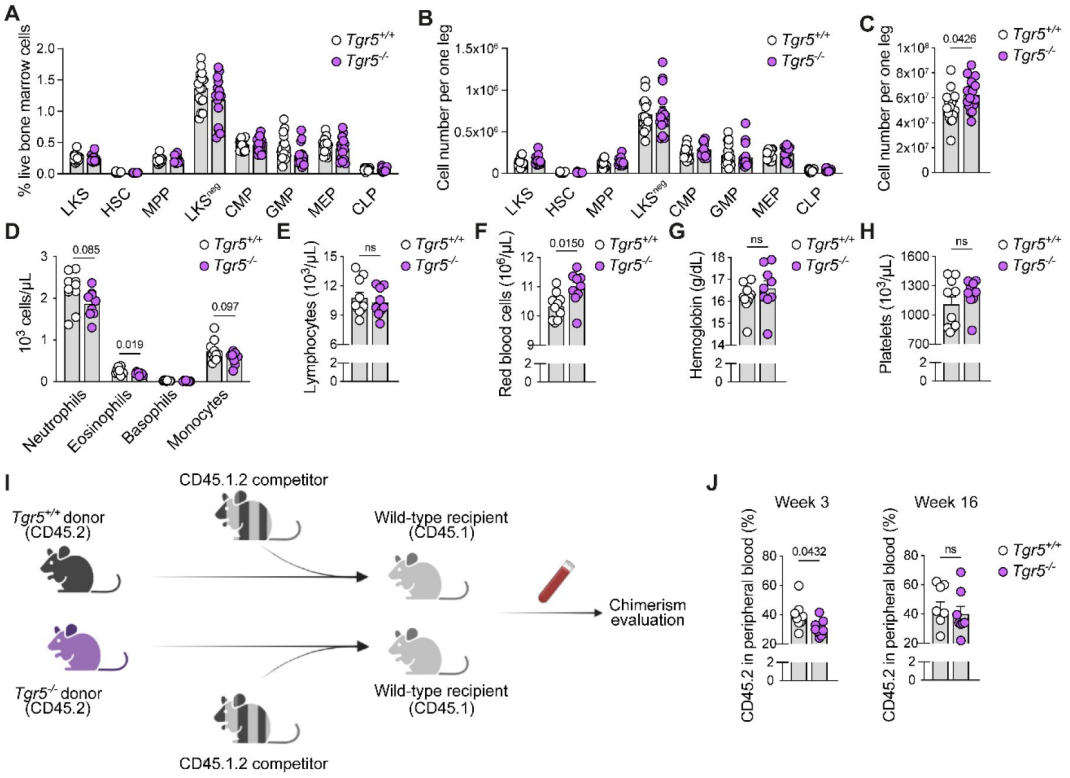

Figure 2.

Loss of TGR5 does not impair steady-state hematopoiesis

A, frequencies of hematopoietic stem and progenitor (HSPCs) populations in the BM of 8-12-week-old *Tgr5*$^{+/+}$ and *Tgr5*$^{-/-}$ male mice expressed as percentage of cells over total live cells acquired (n=16 for *Tgr5*$^{+/+}$ and n= 15 for *Tgr5*$^{-/-}$ mice). **B,** total number of cells per one leg (hip, femur and tibia) for HSPC populations in the BM of 8-12-week-old *Tgr5*$^{+/+}$ and *Tgr5*$^{-/-}$ male mice (n=16 for *Tgr5*$^{+/+}$ and n= 15 for *Tgr5*$^{-/-}$ mice). **C,** total number of CD45^{+} cells per one leg (hip, femur and tibia) in the BM of 8-12-week-old *Tgr5*$^{+/+}$ and *Tgr5*$^{-/-}$ male mice (n=16 for *Tgr5*$^{+/+}$ and n= 15 for *Tgr5*$^{-/-}$ mice). **D-H,** complete blood counts in peripheral blood of 8-12-week-old *Tgr5*$^{+/+}$ and *Tgr5*$^{-/-}$ male mice; myeloid cells (**D**), lymphocytes (**E**), red blood cells (**F**), hemoglobin (**G**), and platelets (**H**). **I,** workflow depicting the primary competitive transplant setting. **J,** flow cytometry analysis of peripheral blood chimerism of serial transplantation experiments (n=8, 8-12-week-old *Tgr5*$^{+/+}$ and *Tgr5*$^{-/-}$ male donors transplanted into 3 CD45.1 recipient mice) at 3 and 16 weeks post-transplant. Axis represents % CD45.2 donor cells over the sum of CD45.2 donor and CD45.1/.2 competitor events (results for secondary and tertiary transplants in supplementary figures). Results represent the mean ± s.e.m., n represents biologically independent replicates Two-tailed Student's t-test was used for statistical analysis. P values (exact value) are indicated, ns indicates non-significance.

parameters were found at the level of the femoral diaphysis (**Fig. S3, A** and **B**), as evaluated by micro-computed tomography (μCT). We could not detect any changes in bone microarchitecture in the spine at the level of L4 in young male *Tgr5*$^{-/-}$ mice (**Fig. S3, C** and **D**). These data suggest that the role of TGR5 on bone microarchitecture differs based on skeletal location, which is in line with the recently described differential regulation of the axial and the appendicular skeleton[43,44].

To further study the overall composition of the BM microenvironment, we used osmium tetroxide (OsO_4) contrast-enhanced μCT[45] to visualize the tibial BMAT. The BMAT in the proximal tibia, also known as regulated BMAT (rBMAT), is regarded as the most dynamic and stimuli-responsive BMAT in opposition to that found in the distal tibia, which is enriched in the less responsive constitutive BMAT (cBMAT)[46]. This analysis revealed a profound reduction in proximal tibia BMAT in young adult *Tgr5*$^{-/-}$ animals as well as a less marked decrease in distal tibia BMAT compared to age-matched controls (*Tgr5*$^{+/+}$) (**Fig. 3**, C and D). As BMAT accumulates with age[47], we evaluated the tibias of 1-year-old *Tgr5*$^{-/-}$ mice, which showed a similar decrease in BMAT compared to their age-matched controls, indicating that the expansion of BMAT with aging was blunted in the absence of TGR5 (**Fig. 3, E** and **F**). Dietary intervention has also been shown to modulate BMAT expansion and high-fat diet (HFD)-feeding robustly increases marrow adiposity, in general, and rBMAT, in particular[13,48,49]. To investigate if TGR5 could control BMAT plasticity upon this intervention, we fed *Tgr5*$^{-/-}$ and *Tgr5*$^{+/+}$ mice with HFD for 8 weeks and evaluated the tibial BMAT. In agreement with our data in young and middle-aged chow-diet (CD)-fed mice (**Fig. 3, C-F**), contrast-enhanced μCT analysis of OsO_4-stained tibias revealed a marked decrease in rBMAT along with a more moderate decrease in cBMAT in *Tgr5*$^{-/-}$ mice compared to their wild-type controls (**Fig. 3, G** and **H**).

Finally, we sought to evaluate whether the robust decrease in rBMAT with a more preserved cBMAT was exclusive of the appendicular skeleton or was also present in axial structures. For this, we chose the caudal spine, as this segment of the vertebral column contains a gradient where rBMAT gives way to cBMAT in a proximal- to-distal manner[47]. μCT scanning of OsO_4-stained caudal spines showed this adipocytic gradient, so-called the yellow-to-red transition. at the level of the second caudal vertebrae (CA2) in young male *Tgr5*$^{+/+}$ mice (**Fig. S3E**). Analogously to our findings for the rBMAT in tibia, *Tgr5*$^{-/-}$ mice presented a marked decrease in BMAT at the level of CA2 (**Fig. S3F, G**). Histological preparations of the same spine segments from an independent cohort further confirmed our μCT data (**Fig. S3H**).

Taken together, our findings indicate a mutual loss of trabecular bone and marrow adiposity in *Tgr5*$^{-/-}$ mice. Specifically, loss of TGR5 decreased trabecular bone in the appendicular skeleton without affecting bone structure at the level of the axial skeleton. Conversely, lack of TGR5 markedly reduced BMAT volume in both the appendicular and axial skeleton. The decrease in BMAT occurred fundamentally at the expense of rBMAT both at homeostasis and under HFD-induced expansion of BMAT, suggesting that TGR5 might be a key player in the regulation of this tissue.

Given the changes in both BMAT and bone architecture, we hypothesized that BM stroma cells (BMSCs) obtained from *Tgr5*$^{-/-}$ mice would present a defect in both adipocytic and osteoblastic differentiation. Surprisingly, and contrary to our hypothesis, *Tgr5*$^{-/-}$ BMSC cultures differentiated better into adipocytes, as evidenced by Oil Red O staining (ORO) (**Fig. 4A**, and **Fig. S4A**) and digital holographic microscopy (**Fig. S4, B** and **C**)[50]. Moreover, *Tgr5*$^{+/+}$ and *Tgr5*$^{-/-}$ BMSCs displayed comparable osteoblastic differentiation, evaluated by alkaline phosphatase staining (ALP) (**Fig. S4D**) and calcium deposition, as evidenced by alizarin red staining (**Fig. S4E**). Taken together, these *in vitro* data indicate that TGR5 deletion does not cause an intrinsic defect in *in vitro* BMSC differentiation.

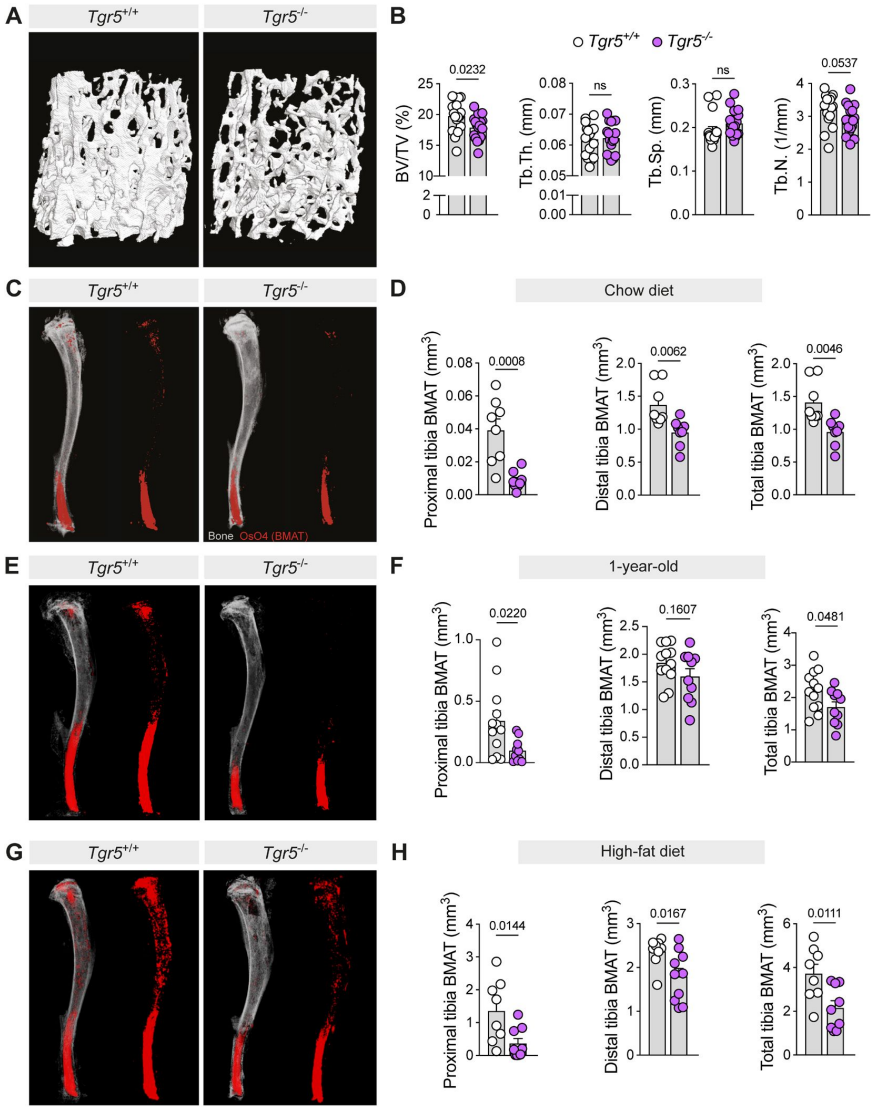

Figure 3.

Loss of TGR5 alters the BM microenvironment

A, representative native µCT-derived 3D reconstructions of the trabecular structure in the distal femoral metaphysis of 8-12-week-old *Tgr5*$^{+/+}$ and *Tgr5*$^{-/-}$ male mice. **B,** µCT-derived bone morphometry measurements of the trabecular structure in the distal femoral metaphysis of 8-12-week-old *Tgr5*$^{+/+}$ and *Tgr5*$^{-/-}$ male mice (n=17 for both *Tgr5*$^{+/+}$ and *Tgr5*$^{-/-}$ mice); shown are bone volume/total volume (BV/TV), trabecular thickness (Tb. Th), trabecular separation (Tb. Sp) and trabecular number (Tb. N) **C,** representative contrast-enhanced µCT-derived 3D reconstructions of osmium tetroxide (OsO_4)-stained BMAT in the tibias of 8-12-week-old *Tgr5*$^{+/+}$ and *Tgr5*$^{-/-}$male mice fed chow diet. **D,** quantification of the OsO_4-stained bone marrow adipose tissue (BMAT) content in chow diet-fed, 8-12-week-old *Tgr5*$^{+/+}$ and *Tgr5*$^{-/-}$ male mice (n=8 for both *Tgr5*$^{+/+}$ and *Tgr5*$^{-/-}$mice). OsO_4-stained BMAT proximal of tibiofibular junction was classified as "proximal BMAT"; OsO_4-stained BMAT distal of tibiofibular junction was classified as "distal BMAT". **E,** representative contrast-enhanced µCT-derived 3D reconstructions of OsO_4-stained BMAT in the tibias of 1-year-old *Tgr5*$^{+/+}$ and *Tgr5*$^{-/-}$ male mice. **F,** quantification of the OsO_4-stained BMAT content in 1-year-old *Tgr5*$^{+/+}$ and *Tgr5*$^{-/-}$ male mice (n=12 for *Tgr5*$^{+/+}$ and n=10 for *Tgr5*$^{-/-}$ mice). Proximal and distal BMAT were defined as in D. **G,** representative contrast-enhanced µCT-derived 3D reconstructions of OsO_4-stained BMAT in the tibias of 20-week-old *Tgr5*$^{+/+}$ and *Tgr5*$^{-/-}$male mice fed high-fat diet. **H,** quantification of the OsO_4-stained BMAT content in 20-week-old *Tgr5*$^{+/+}$ and *Tgr5*$^{-/-}$male mice fed for 12 weeks with high-fat diet (n=8 for both *Tgr5*$^{+/+}$ and *Tgr5*$^{-/-}$ mice). Proximal and distal BMAT were defined as in D. Results represent the mean ± s.e.m., n represents biologically independent replicates. Two-tailed Student's t-test **(B, D, F, H)** was used for statistical analysis. P values (exact value) are indicated, ns indicates no statistical significance.

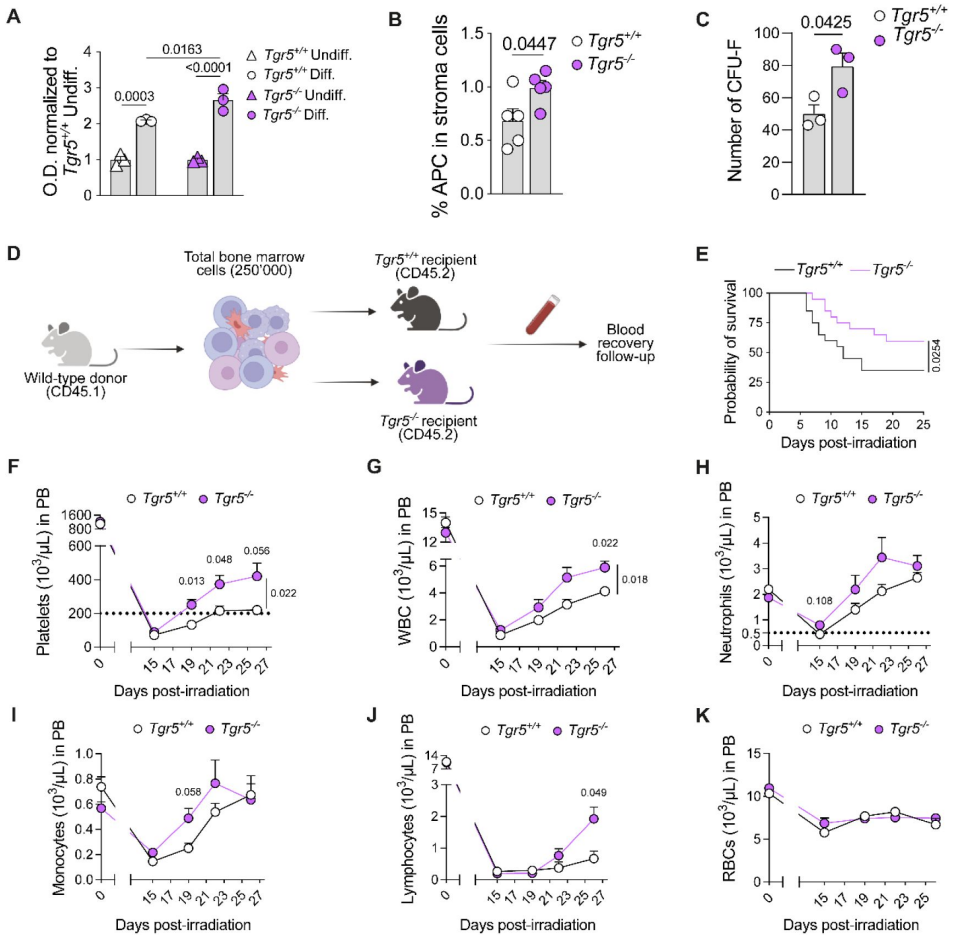

Figure 4.

Loss of TGR5 leads to accumulation of adipocyte progenitors and hastens hematopoietic recovery upon irradiation and BM transplantation

A, spectrophotometric quantification of Oil red O (ORO)-stained BMSCs after 7 days of adipocytic differentiation (n=3 for both *Tgr5*$^{+/+}$ and *Tgr5*$^{-/-}$). **B,** percentage of adipocyte progenitor cells (APCs) in the CD45^{-}Ter119^{-}CD31^{-} BM stromal gate (n=5 for both*Tgr5*$^{+/+}$ and *Tgr5*$^{-/-}$). **C,** number of fibroblast colony-forming units (CFU-Fs) obtained from 1 million total BM cells (n=3 both for *Tgr5*$^{+/+}$ and *Tgr5*$^{-/-}$). **D,** Schematic depiction of the inverse chimera transplantation setup. **E,** survival of BM transplant recipients (n=20 for both *Tgr5*$^{+/+}$ and *Tgr5*$^{-/-}$ at D0, 8-12-week-old male mice in 2 independent experiments). **F-K** peripheral blood recovery evaluated longitudinally by complete blood counts for platelets (**F**), white blood cells (WBCs) (**G**), neutrophils (**H**), monocytes (**I**), lymphocytes (**J**) and red blood cells (RBCs) (**K**) (n=7 for *Tgr5*$^{+/+}$ and n=12 *Tgr5*$^{-/-}$ 8-12-week-old male recipient mice). Results represent the mean ± s.e.m. All *in* vitro experiments were conducted on cells obtained from 8-12-week-old *Tgr5*$^{+/+}$ and *Tgr5*$^{-/-}$ male mice. One-way ANOVA with Bonferroni multiple test correction (**A**), two-tailed Student's t-test (**B, C**), Mantel-Cox test (**E**) and two-way ANOVA with Holm-Šídák multiple comparison correction (**F-K**) were used for statistical analysis. For E, baseline values (Day 0) were not considered for the analysis of the recovery. P values (exact value) are indicated, ns indicates non-significance

Recent reports have revealed that lipodystrophy or specific ablation of pre-adipocytic populations in the BM leads to massive trabecular bone invasion of the medullary cavity, indicating that these populations negatively regulate the mineralized compartment of the BM microenvironment[4,6–8,42,51,52]. Considering this, we hypothesized that our findings in *Tgr5*$^{-/-}$ mice, (i.e., decreased BMAT and trabecular bone together with an increased *in vitro* adipocyte differentiation), could be explained by an *in vivo* blockage of lipidation of adipocyte progenitor cells (APCs) that is rescued upon forced induction of *in vitro* adipocytic differentiation. In order to assess this, we analyzed the BM stroma based on the expression of Sca1 and CD24 for APC quantification[13]. In agreement with our hypothesis, we found an increase in immunophenotypic APCs (CD45^{-}Ter119^{-}CD31^{-}Sca1^{+}CD24^{-}) in the stroma of *Tgr5*$^{-/-}$ mice (**Fig. 4B**, and **Fig. S4F**). Finally, we observed an alteration in the clonogenic capacity of BMSCs, evidenced by an increase in fibroblast colony-forming units (CFU-F) in *Tgr5*$^{-/-}$ BM and compared to wildtype controls (**Fig. 4C**, and **Fig. S4G**), which agrees with a shift towards less differentiated BM stromal populations in *Tgr5*$^{-/-}$ animals. Taken together, our findings indicate that TGR5 loss-of-function perturbs the bone-BMAT-hematopoietic tissue equilibrium within the marrow cavity and suggests that TGR5 signaling is necessary for BM pre-adipocytes to fully mature.

Given the accumulation of APCs in *Tgr5*$^{-/-}$ mice, we next investigated the impact of the associated BM microenvironment alterations in stress hematopoiesis. Based on the first report of the negative effect of lipidated BM adipocytes on hematopoietic recovery[4] and recent work showing that non-lipidated adipocytic precursors improve hematopoietic recovery[16], we reasoned that the displacement of the BM adipocyte differentiation axis towards non-lipidated progenitors observed in the BM microenvironment of *Tgr5*$^{-/-}$ mice would correlate with an improved early hematopoietic recovery upon irradiation and transplantation. To assess this, we generated inverse chimeras (**Fig. 4D**) and evaluated early hematopoietic recovery using CBCs as a direct readout of the functionality of the system for the first 4 weeks post-irradiation. We observed lower mortality post-transplant in the *Tgr5*$^{-/-}$ recipients (**Fig. 4E**) and faster hematopoietic recovery in *Tgr5*$^{-/-}$ recipients upon lethal irradiation and transplantation with wild-type donor cells. *Tgr5*$^{-/-}$ recipients recovered their platelet levels faster than the *Tgr5*$^{+/+}$ recipients, showing values consistently above 200.000/µL one week sooner; platelet levels below this threshold are considered a risk factor for bleeding events (**Fig. 4F**)[53,54]. The recovery was also faster for white blood cells (WBCs) (**Fig. 4G**) without a clear predominance of any cell type as shown for neutrophils (**Fig. 4H**), monocytes (**Fig. 4I**) or lymphocytes (**Fig. 4J**). Of note, *Tgr5*$^{-/-}$ recipients had their neutrophil levels over 500.000 cells/µL, the threshold value for infection risk[53,54], on day 15 post-irradiation (uncorrected p-value 0.028) but this difference was no longer statistically significant upon multiple-comparison correction. We observed no major differences in the recovery of red blood cells (**Fig. 4K**). Taken together, our findings suggest that the loss of TGR5 leads to a BM stroma that is beneficial for early hematopoietic recovery.

Discussion

In the current study, we aimed at investigating the role of TGR5 on BM homeostasis. We showed that TGR5 loss-of-function leads to the accumulation of adipocytic precursors and a simultaneous loss of BMAT, suggesting that TGR5 is necessary for the *in vivo* maturation of BM adipocytes in young male mice. We also found that *Tgr5*$^{-/-}$ mice receiving BM transplantation after lethal irradiation recover faster than their *Tgr5*$^{+/+}$ counterparts, which could be a consequence of the accumulation of adipocyte precursors[16], a decrease of lipidated adipocytes[4], or a combination of both.

The BM adipocyte differentiation axis is gaining attention as a fundamental component of bone and blood physiology, with several recent studies focusing on the BM stroma population as a key player in the maintenance of the balance between bone and BM space[8,55]. Ablation of the BM

adipocyte precursor population leads to massive accumulation of bone in the medullary cavity[4,7,14,52,54] which in turn reduces the volume available for hematopoietic tissue. In agreement with this model, we observe that male *Tgr5*$^{-/-}$ mice display an increase in adipocytic precursors, a decrease in bone, and an expansion of CD45^{+} cells in the BM.

BMAT has been described as a highly dynamic fat depot that responds to dietary changes, but it has distinct characteristics compared with extramedullary fat, both from a biological and regulatory perspective[56]. For instance, and surprisingly, both nutrient deprivation (e.g. caloric restriction and anorexia) and excess (e.g. HFD feeding) result in BMAT expansion[49,57–59]. Although counterintuitive, this nutrient-mediated control of BMAT ensures energy conservation in BM to support the energy-consuming process of hematopoiesis and bone remodeling[60,61]. Another difference between BMAT and peripheral adipose tissues is the absence of HFD-induced pro-inflammatory response in the BMAT compared with the latter[49]. While the role of TGR5 in extramedullary adipose tissues has been extensively studied, and shown to be important for beige remodeling[31,32], lipolysis[32], and protection against diet-induced immune infiltration of the white adipose tissue[29,33], the effects of an activated TGR5 signaling pathway in BMAT and its impact on hematopoiesis is unknown and will require future investigation. Of note, the BA ursodeoxycholic acid (UDCA) is routinely used in clinics in the context of BM transplantation, where supplementation with UDCA has been shown to reduce post-transplant complications and improve overall survival[62]. Available reports have attributed these benefits to the unique feature of tauro-conjugated form of UDCA (TUDCA) as chemical chaperones, improving protein folding in fetal liver HSCs[38] or after acute BM insult[39]. In addition, UDCA and TUDCA are hydrophilic BAs, and part of their beneficial effects could be a consequence of changes in the hydrophobicity of the BA pool[63,64]. However, BAs signal through dedicated BA receptors, but the receptor-mediated signaling of UDCA and TUDCA remains unclear. Although some studies proposed UDCA as a TGR5 agonist[65–68], effects occur mainly at supra-physiological doses of UDCA. In addition, the EC_{50} of UDCA for TGR5 is more than 60 times higher than that of the strongest endogenous TGR5 agonist, lithocholic acid (LCA)[69], indicating that UDCA is a poor TGR5 agonist. Based on this notion, it will be interesting to investigate whether, in these context-dependent conditions, the benefits of UDCA upon stress hematopoiesis result from the inability to activate TGR5 signaling in the BMAT. Future work will be needed to confirm this possibility.

Finally, novel therapeutic strategies could be envisioned in the future to pharmacologically mimic TGR5 inhibition in the BMAT. Although several selective TGR5 agonists have been developed, only a few TGR5 antagonists have been discovered, namely triamterene[70] and SBI-115[71]. However, these compounds have only been used *in vitro,* and additional *in vivo* research and optimization will be required to pharmacologically block TGR5 in the context of hematopoietic stem cell transplantation or other conditions linked to stress hematopoiesis, in which a fast production of mature blood cells is required. Our results indicate that deletion of TGR5 modulates the BM adipocyte lineage and suggest that strategies aimed at blocking the activity of this receptor might be therapeutically attractive.

Author contribution

AAC, AP and FS: Data curation, Formal analysis, Investigation, Methodology, Writing – original draft, writing – review and editing. SFL, VD, AJ, UK, DPP: Methodology. KS and ON Conceptualization, Resources, Supervision, Funding acquisition, Validation, Investigation, Writing – original draft, Project administration, Writing – review and editing.

Acknowledgements

We wish to thank the Histology Core Facility, Center for Phenogenomics, Bioscreening Facilities, Electron Microscopy facilities and BioImaging and Optics Platform at EPFL as well as the In Vivo Imaging Facilities at AGORA (UNIL/EPFL) and Flow Cytometry facilities at AGORA (UNIL/EPFL) for their continuous support and guidance for this project. This work was funded by the Ecole Polytechnique Fédérale de Lausanne (EPFL), the University of Lausanne (UNIL), the Swiss National Science Foundation (SNSF N° 310030_189178, Sinergia CRSII5_180317/1 to K.S. and SNSF Professorship grant PP00P3_144857 and 183725 to O.N.), and La Caixa Foundation (to K:S). Alessia Perino was supported by a fellowship from AXA Research Fund. Frédérica Schyrr was funded by the SNSF MD-PhD grant 183986.

Materials and Methods

Animal studies

Generation of mouse models and tissue collection

To evaluate the expression of TGR5 in peripheral blood and BM, we used a transgenic mouse reporter model (TGR5:GFP), that co-expresses human TGR5 and the enhanced green fluorescent protein (GFP) linked by the foot-and-mouth disease virus (*F2a*) cleaving peptide sequence under the control of the endogenous *Tgr5* mouse promoter [41,72].

Mice were housed with ad libitum access to water and food and kept under a 12-h dark/12-h light cycle with a temperature of 22 °C ± 1 °C and a humidity of 60% ± 20%. 8- to 12-week-old male mice fed chow diet (CD, SAFE 150) were used for all experiments. 1-year-old male mice fed (CD, SAFE 150) were used where indicated. For the high-fat diet experiment, 8-week-old male mice were fed HFD (Research Diets D12492) for 12 weeks. The whole-body TGR5 knock-out mouse model ($Tgr5^{-/-}$) has been previously described [73]. C57BL/6J (CD45.2) and C57BL/6J Ly5.1 (CD45.1) mice were bred in-house at the EPFL facility. Double congenic mice (CD45.1/.2) were bred in-house, by crossing CD45.2 and CD45.1 mice.

BM transplantation

For transplantation assays, recipient mice were irradiated (lethal x-ray irradiation 8.5 Gy, split in two 4.25 Gy doses 4 h apart using an RS-2000 X-ray irradiator (RAD SOURCE). Transplanted cells were administered the day following irradiation via tail-vein injection. For two weeks after lethal irradiation, mice were treated in drinking water with paracetamol (500 mg Dafalgan in 250 ml water). No antibiotics were provided in drinking water. For the primary competitive transplant setting, 300.000 cells of each the CD45.2 donor ($Tgr5^{-/-}$ or $Tgr5^{+/+}$) and the CD45.1/.2 competitor were co-administered. For the secondary and tertiary transplant, 4 million cells were collected from the primary donor and transplanted into the recipient. For the inverse chimera experiments where the CD45.2 mice were the recipients ($Tgr5^{-/-}$ or $Tgr5^{+/+}$), 250.000 CD45.1 total BM cells were administered.

Blood collection for the experiments described in this work was performed at noon. Blood was obtained from the tail vein by means of a small incision with a scalpel blade and collected into EDTA-coated tubes. Complete blood counts were obtained with an Element HT5 hematology analyzer (Heska, USA)

μCT analysis

To evaluate bone microarchitecture and osmium tetroxide (OsO_4) stains, a SkyScanner 1276 (Bruker, Belgium) was used. For both applications, an 0.25 mm Al filter was used with a voltage of 200 kV and a current of 55 mA. Samples were wrapped in PBS-soaked paper towels and scanned inside a drinking straw sealed on both ends to avoid drying. Voxel size for both applications was set at 10×10×10 μm^3.

Bone microarchitecture was evaluated according to the ASBMR guidelines [74] using a custom CTan (Bruker, Belgium) script for automatic segmentation of trabecular bone in the distal femoral VOI, which was set 100 slices proximal to the distal growth plate and extended 200 slices towards the femoral diaphysis (slice thickness of 0.010 mm). The threshold used to binarize the calcified tissue was 40 on a 0-255 scale. Reconstruction of the scans was performed using NRecon (Bruker, Belgium) and further analysis were performed using CTan (Bruker, Belgium) with the minimum for CS to image conversion set at 0 and maximum set at 0.14. For the analysis of cortical parameters, the midpoint of the femur was determined, and the VOI was defined as the bone 50 slices (slice thickness of 0.010 mm) distal and proximal of the slice corresponding to the midpoint of the bone. All other parameters were kept the same as for the analysis of trabecular bone.

OsO_4 stained was performed on formalin-fixed, EDTA-decalcified tibias. For this, tibias were kept in 10% formalin for 24 hours at 4 °C. Following fixation, the bones were decalcified in PBS-0.5 M EDTA for 2 weeks refreshing of the decalcifying solution on day 7. OsO_4-was performed as previously described [45]. Reconstruction of the scans was performed as for calcified bone except for the minimum and maximum CS range, which was set to 0 and 0.30, respectively. OsO_4 was segmented using a threshold of 50 on a 0-255 scale. Images and quantification of BMAT were analyzed using Dragonfly software (ORS, Canada).

Flow cytometry

All antibodies used for this work as well as their dilutions are listed in **Supplementary Table 1**. All dilutions and cell suspensions were prepared in FACS buffer (2% serum + 1 mM EDTA in PBS).

Histology

Spleens and thymus were fixed in 10% formalin for 24 h at 4 °C. EDTA-decalcified bones (as described previously for OsO_4 stain), spleens and thymus were cut longitudinally in 3-4 μm sections for staining. For IHC, detection of rabbit anti-GFP (Abcam, ab6673,) was performed manually. After quenching with 3% H_2O_2 in PBS 1x for 10 min, a heat pretreatment using 0.1 M Tri-Na citrate pH 6 was applied at 60 °C in a water bath overnight. Primary antibodies were incubated overnight at 4 °C. After incubation of ImmPRESS HRP (Ready to use, Vector Laboratories), revelation was performed with DAB (3,3'-Diaminobenzidine, D5905, Sigma-Aldrich). Sections were counterstained with Harris hematoxylin and permanently mounted. All slides were imaged on an automated slide scanner (Olympus VS120-SL) at 20x or 40x.

Cell culture

Cell extraction

Culture of primary BMSCs was performed as reported in the literature [75]. 8-12-week-old male mice were used for these experiments. To isolate BMSCs from the BM, we collected femora and tibias, cut the epiphyses, and placed the bones in a 200 μL pipette tip with its end cut to fit in a 1.5 mL microcentrifuge tube. Bones were spun at 10.000 g for 10 seconds to flush out the BM from the medullary cavity. The BM plug was then transferred to a 15 mL conical tube containing 10 mL of ascorbic-acid free αMEM (containing 10% FBS and 1% penicillin-streptomycin) and this

suspension filtered through a 70 µm mesh filter prior to plating in a 100 mm cell culture dish (Corning, USA). Cells were replated 72 hours later at a density of 62.500 cells/cm^2 in tissue-culture treated 12-well plates (i.e., 250.000 cells/well) and grown to confluency prior to differentiation. Culture medium was refreshed every other day until confluency[75].

For CFU-F assays, BM was obtained in a similar manner and plated at a density of 1 million cells per well of a tissue-culture treated 6-well plate (i.e., 100.000 cells/cm^2). CFU-F cultures were kept in αMEM containing 10% FBS and 1% penicillin-streptomycin and stained on day 7 post-plating with 0.1% toluidine blue in 10% formalin.

Media composition and differentiation cocktail

Differentiation into osteoblasts was started once confluency was reached. For osteoblastic differentiation, the base culture medium of ascorbic-acid free αMEM containing 10% FBS and 1% penicillin-streptomycin was supplemented with L-ascorbic acid (final concentration 8 mM) and β-glycerophosphate (final concentration 1 mM) and refreshed every other day until the endpoint of the assay.

Differentiation into adipocytes was started once confluency was reached. For adipocytic differentiation, base culture medium was high-glucose (4.5 g/L) DMEM supplemented with 10% FBS and 1% penicillin-streptomycin was used. Adipocytic induction medium containing dexamethasone (1 µM), isobutylmethylxanthine (IBMX, 0.5 mM), insulin (2 µM) and rosiglitazone (20 µM) was prepared. Cells were cultured in adipocytic differentiation medium for 4 days with refreshing on day 2. On day 4, culture medium was changed to maintenance medium, prepared by supplementing the base medium with only insulin (2 µM) and rosiglitazone (20 µM). Cells were kept in maintenance medium until the endpoint (Day 7 post-differentiation) with no medium refreshing.

Differentiation stains

For alkaline phosphatase (ALP) stain of osteoblast cultures, one tablet of SigmaFast (Sigma-Aldrich) was dissolved in 10 mL distilled water. Osteoblasts were fixed in 10% formalin for 1 minute, washed once with PBS-0.05% Tween 20 and incubated in the staining solution for 6 minutes. Cells were then washed with PBS-0.05% Tween 20 and imaged.

For alizarin red (AR) stain of calcium deposits in osteoblastic cultures after ALP staining, cells were washed once with distilled water and incubated for 45 minutes with AR stain (prepared fresh with 2 g of alizarin red in 100 mL distilled water and pH adjusted to 4.2). Cells were then washed with distilled water 4 times and imaged.

For Oil Red O (ORO) staining of adipocyte cultures, we fixed the cells in 10% formalin for 1 hour at room temperature. In the meantime, we filtered the ORO stock solution through filter paper as described in the literature [75]. Cells were stained with ORO for 15 minutes, washed 6 times with distilled water, imaged, and incubated for 10 minutes with 100% isopropanol to solubilize the stain. ORO was quantified using an iD3 plate reader (Agilent, USA) set to measure absorbance at 490 nm [75].

Digital holographic microscopy

Digital holographic imaging was performed in black wall 96-well imaging plates (Corning, 353962) using Transmission DHM® T1000 (Lyncée Tec, Switzerland). Plates were pre-coated with Poly-ornithine (Sigma,100 mg/L) to prevent cell detachment. The cells were imaged live and without prior liquid manipulation using a 20x/0.4 NA microscope objectives. The best-focus phase images

were reconstructed automatically in MATLAB (MathWorks, USA) from the acquired holograms and the average quantitative phase signal or optical path difference (OPD) was automatically measured using a fixed threshold value.

Ethical approval

Experiments were carried out in accordance with the Swiss law and with approval of the cantonal authorities (Service Vétérinaire de l'Etat de Vaud, authorization nos. 2990, 2990.1, 2990.2 and 3740). No statistical methods were used to predetermine sample size. Mice were randomly assigned to control and intervention groups. The investigators were not blinded to allocation during experiments and outcome assessment unless otherwise stated.

Statistics

Differences in groups were assessed as stated in the legend for each figure. GraphPad Prism 9 was used for all statistical analyses. The studies were either replicated and/or the results were confirmed by using different approaches (flow cytometry and immunohistochemistry, for example) yielding similar results. All P values ≤ 0.05 were considered significant. When the exact value is not provided, *P ≤ 0.05, **P ≤ 0.01, ***P ≤ 0.001 and ****P ≤ 0.0001.

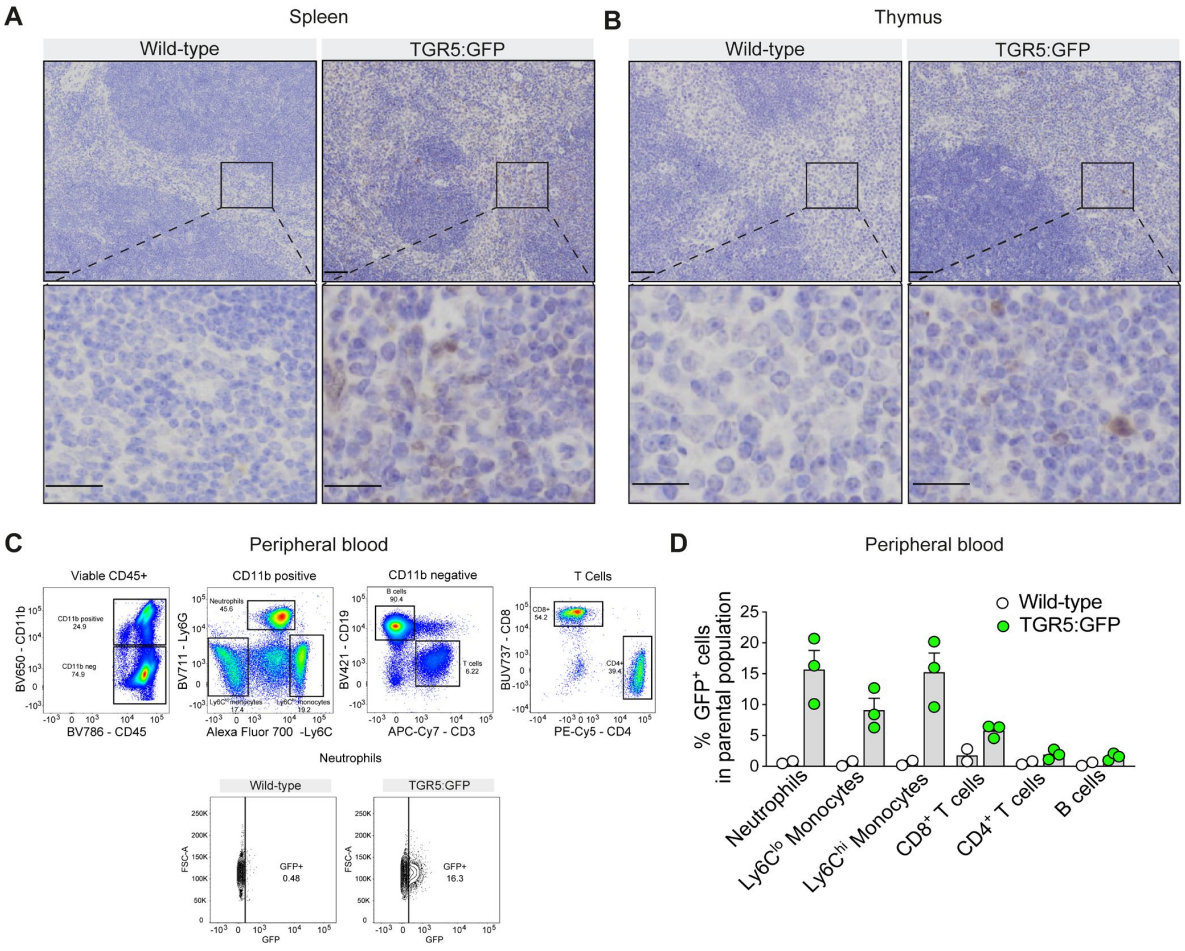

Figure S1.

TGR5 is expressed in spleen, thymus and differentiated hematopoietic populations

A, B, immunodetection of GFP$^+$ cells by DAB immunohistochemistry in spleen (**A**) and thymus (**B**) of 8-12-week-old male TGR5:GFP mice (n=2 for wild-type control mice, n=3 for TGR5:GFP mice). Scale bar: 50 μm in low magnification images, 20 μm in the corresponding digitally zoomed images. **C,** representative flow cytometry gating strategy used to identify differentiated population in peripheral blood and GFP positivity in TGR5:GFP mice. **D**, frequencies of GFP$^+$ cells in peripheral blood cell populations of 8-12-week-old male TGR5:GFP mice and their wild-type controls (n=2 for wild-type control mice, n=3 for TGR5:GFP mice, axis represents % GFP$^+$ cells within the viable CD45$^+$ cell gate) Results represent the mean ± s.e.m., n represents biologically independent replicates.

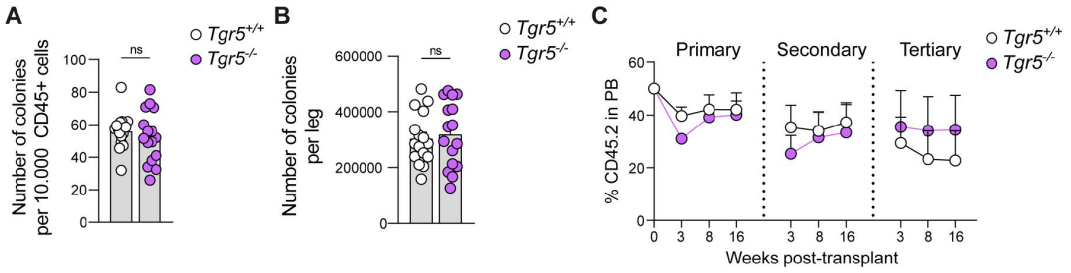

Figure S2.

Loss of TGR5 does not impair steady-state hematopoiesis

A, number of colonies per 10.000 total BM CD45^{+} cells (**A**) and per leg (**B**) (n=16 for *Tgr5*$^{+/+}$ and n= 15 for *Tgr5*$^{-/-}$ mice). **C,** flow cytometry analysis of peripheral blood chimerism of serial BM transplantation experiments (n=8, 8-12-week-old *Tgr5*$^{+/+}$ and *Tgr5*$^{-/-}$ male donors transplanted into 3 CD45.1 recipient mice each) at 3 and 16 weeks post-transplant. Results represent the mean ± s.e.m., n represents biologically independent replicates Two-tailed Student's t-test was used for statistical analysis. ns indicates non-significance.

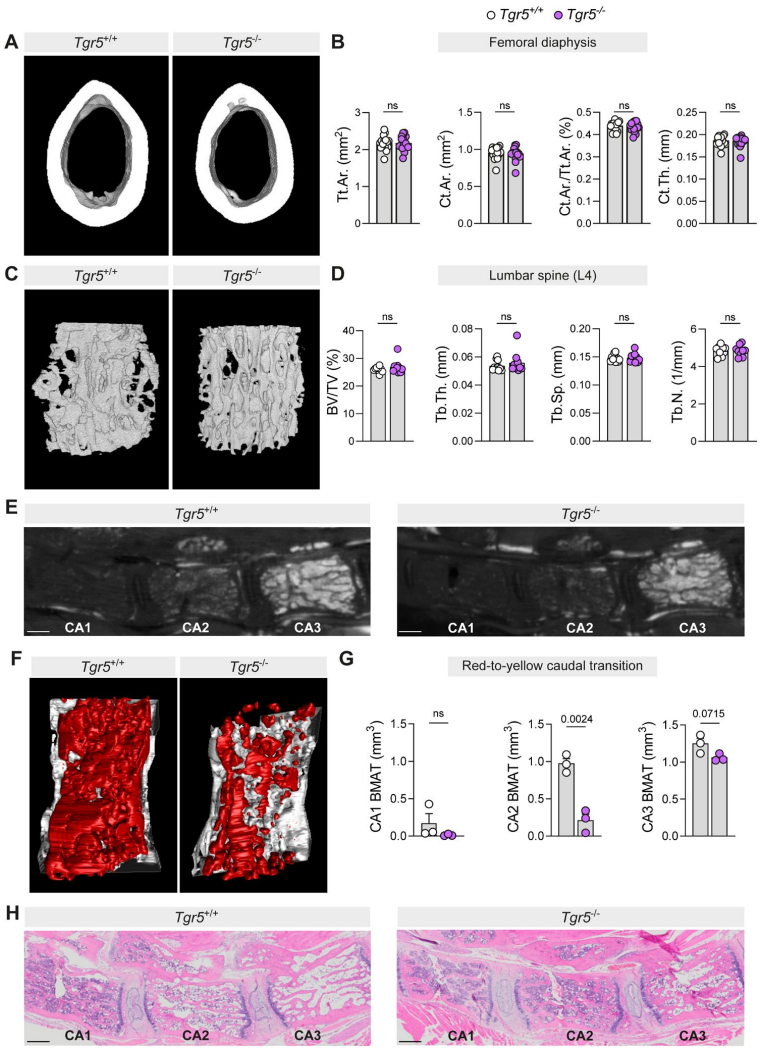

Figure S3.

Loss of TGR5 alters the BM microenvironment

A, representative native µCT-derived 3D reconstructions of the cortical bone in the mid-femoral diaphysis of 8-12-week-old *Tgr5*$^{+/+}$ and *Tgr5*$^{-/-}$ male mice. **B,** µCT-derived bone morphometry measurements of the cortical bone in the mid-femoral diaphysis of 8-12-week-old *Tgr5*$^{+/+}$ and *Tgr5*$^{-/-}$ male mice (n=17 for both *Tgr5*$^{+/+}$ and *Tgr5*$^{-/-}$ mice); shown are the total cross-sectional area inside the periosteal envelope (Tt.Ar), cortical bone area (Ct.Ar), cortical area fraction (Ct.Ar/Tt.Ar) and average cortical thickness (Ct. Th). **C,** representative native µCT-derived 3D reconstructions of the trabecular structures in the fourth lumbar vertebrae (L4) of 8-12-week-old *Tgr5*$^{+/+}$ and *Tgr5*$^{-/-}$ male mice. **D,** µCT-derived bone morphometry measurements of the trabecular structures in L4 of 8-12-week-old *Tgr5*$^{+/+}$ and *Tgr5*$^{-/-}$ male mice (n=17 for both *Tgr5*$^{+/+}$ and *Tgr5*$^{-/-}$ mice); shown are bone volume/total volume (BV/TV), trabecular thickness (Tb. Th), trabecular separation (Tb. Sp) and trabecular number (Tb. N). **E**, representative images obtained from contrast-enhanced µCT scanning of decalcified OsO_4-stained spines depicting lipid content in the red-to-yellow marrow transition in the caudal spine (CA) of 12-week-old male *Tgr5*$^{+/+}$ and *Tgr5*$^{-/-}$ mice. **F,** sagittal view of a representative µCT-derived 3D reconstructions of OsO_4-stained BMAT in the second caudal vertebrae (CA2) of 12-week-old *Tgr5*$^{+/+}$ and *Tgr5*$^{-/-}$male mice fed chow diet. **G,** quantification of the OsO_4-stained BMAT for the first to third caudal vertebra (CA1-CA3) in the caudal red-to-yellow transition in chow diet-fed, 12-week-old *Tgr5*$^{+/+}$ and *Tgr5*$^{-/-}$ male mice (n=3 for both *Tgr5*$^{+/+}$ and *Tgr5*$^{-/-}$ mice). Results represent the mean ± s.e.m., n represents biologically independent replicates. **H**, representative hematoxylin & eosin (H&E) histological sections of CA1-CA3 from a cohort independent from the animals shown in **E** (n=4 for both *Tgr5*$^{+/+}$ and *Tgr5*$^{-/-}$ mice). Scale bar in **E** and **H** = 500 µm. Results represent the mean ± s.e.m., n represents biologically independent replicates. Two-tailed Student's t-test **(B, D, G)** was used for statistical analysis. P values (exact value) are indicated, ns indicates no statistical significance.

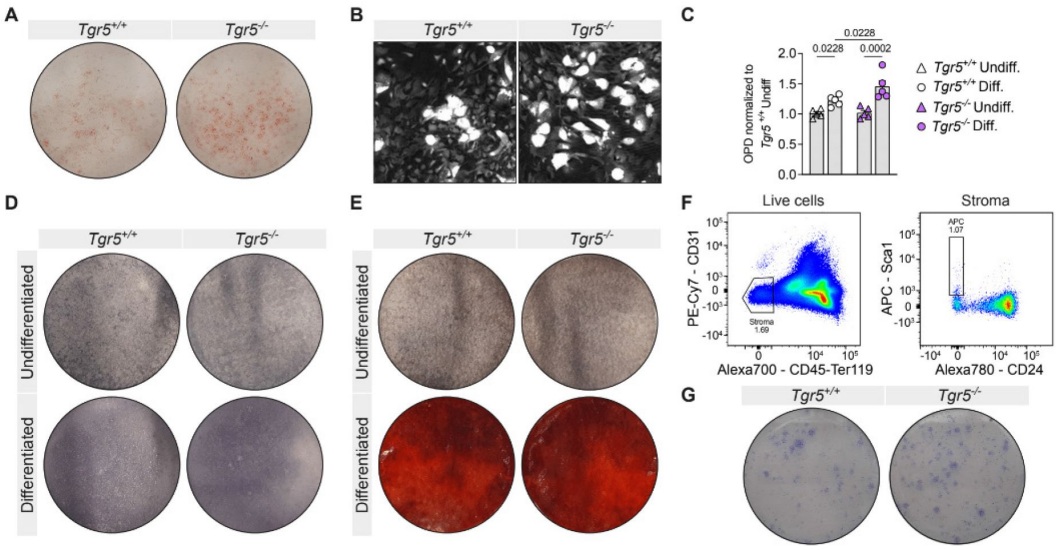

Figure S4.

Loss of TGR5 leads to accumulation of adipocyte progenitors

A, representative images of Oil red O (ORO)-stained BMSCs after 7 days of adipocytic differentiation. **B-C,** digital holographic microscopy imaging of BMSCs after 7 days of adipocytic differentiation. Optical path difference (OPD) quantification, indicative of the degree of lipidation (**B**) and representative images; lipid inclusions appear as bright areas in this technique (**C**). **D-E,** alkaline phosphatase (ALP) (**D**) and alizarin red (AR) (**E**) on top of ALP stains of BMSCs after 7 days of osteoblastic differentiation. **F**, representative flow cytometry gating strategy for the CD45-Ter119-CD31-BM stroma population and adipocyte progenitor cells (APCs) in the BM stroma gate. **G**, representative images for fibroblast colony-forming units (CFU-F) assay. All cells were obtained from 8-12-week-old *Tgr5*$^{+/+}$ and *Tgr5*$^{-/-}$ male mice. One-way ANOVA with Holm-Šídák multiple test correction (**B**) was used for statistical analysis. P values (exact value) are indicated.

Antibodies flow cytometry (anti-mouse)	Commercial source	Cat.no
Biotin lineage cocktail	BD Biosciences	51-9000724
Streptavidin - Texas Red	Invitrogen	S872
cKit - PE/Cy7	Biolegend	105814
Sca1 - BV711	BD Biosciences	563992
CD150 - PE/Cy5	Biolegend	115912
CD48 - Pacific Blue	Biolegend	103418
CD34 - eFluor 660	Invitrogen	50-0314-82
CD127 - PE	Invitrogen	12-1271-83
CD16/32 - Alexa Fluor700	Invitrogen	56-0161-82
Sca1 - APC	Biolegend	105112
PDGFRa - PE	Biolegend	135905
CD45 - Alexa Fluor700	Biolegend	103128
Ter119 - Alexa Fluor 700	Biolegend	116220
CD24 APC eFluor780	Invitrogen	47-0242-82
CD31 - PE/Cy7	Biolegend	102418
CD45 - BV785	Biolegend	103149
CD11b - BV650	Biolegend	101239
Ly6G - BV711	Biolegend	127643
Ly6C - Alexa Fluor 700	Biolegend	128024
CD4 - PE/Cy5	Biolegend	100410
CD19 - BV421	BD Biosciences	562440
CD8 - BUV737	BD Biosciences	612759
CD3 - APC/Cy7	Biolegend	100222

Supplementary table 1.

List of antibodies used in flow cytometry experiments

References

1. Pinho S., Frenette P. S (2019) **Haematopoietic stem cell activity and interactions with the niche** *Nat. Rev. Mol. Cell Biol* **20**:303–320

2. Bolamperti S., Villa I., Rubinacci A (2022) **Bone remodeling: an operational process ensuring survival and bone mechanical competence** *Bone Res* **10**

3. Baccin C., et al. (2020) **Combined single-cell and spatial transcriptomics reveal the molecular, cellular and spatial bone marrow niche organization** *Nat. Cell Biol* **22**:38–48

4. Naveiras O., et al. (2009) **Bone-marrow adipocytes as negative regulators of the haematopoietic microenvironment** *Nature* **460**:259–263

5. Zhou B. O., et al. (2017) **Bone marrow adipocytes promote the regeneration of stem cells and haematopoiesis by secreting SCF** *Nat. Cell Biol* **19**:891–903

6. Yu W., et al. (2021) **Bone marrow adipogenic lineage precursors promote osteoclastogenesis in bone remodeling and pathologic bone loss** *J. Clin. Invest* **131**

7. Zhong L., et al. (2020) **Single cell transcriptomics identifies a unique adipose lineage cell population that regulates bone marrow environment** *eLife* **9**

8. Zhong L., et al. (2023) **Csf1 from marrow adipogenic precursors is required for osteoclast formation and hematopoiesis in bone** *eLife* **12**

9. Wilson A., Trumpp A. (2006) **Bone-marrow haematopoietic-stem-cell niches** *Nat. Rev. Immunol* **6**:93–106

10. Gomariz A., et al. (2018) **Quantitative spatial analysis of haematopoiesis-regulating stromal cells in the bone marrow microenvironment by 3D microscopy** *Nat. Commun* **9**

11. Morrison S. J., Scadden D. T (2014) **The bone marrow niche for haematopoietic stem cells** *Nature* **505**:327–334

12. Zhu R.-J., Wu M.-Q., Li Z.-J., Zhang Y., Liu K.-Y (2013) **Hematopoietic recovery following chemotherapy is improved by BADGE-induced inhibition of adipogenesis** *Int. J. Hematol* **97**:58–72

13. Ambrosi T. H., et al. (2017) **Adipocyte Accumulation in the Bone Marrow during Obesity and Aging Impairs Stem Cell-Based Hematopoietic and Bone Regeneration** *Cell Stem Cell* **20**:771–784

14. Wilson A., et al. (2018) **Lack of Adipocytes Alters Hematopoiesis in Lipodystrophic Mice** *Front. Immunol* **9**

15. Sato K., et al. (2016) **PPAR antagonist attenuates mouse immune-mediated bone marrow failure by inhibition of T cell function** *Haematologica* **101**:57–67

16. Zhong L., et al. (2022) **Transient expansion and myofibroblast conversion of adipogenic lineage precursors mediate bone marrow repair after radiation** *JCI Insight* **7**

17. Cawthorn W. P., et al. (2016) **Expansion of Bone Marrow Adipose Tissue During Caloric Restriction Is Associated With Increased Circulating Glucocorticoids and Not With Hypoleptinemia** *Endocrinology* **157**:508–521

18. Tavassoli M (1974) **Differential response of bone marrow and extramedullary adipose cells to starvation** *Experientia* **30**:424–425

19. Ackert-Bicknell C. L., et al. (2009) **Strain-Specific Effects of Rosiglitazone on Bone Mass, Body Composition, and Serum Insulin-Like Growth Factor-I** *Endocrinology* **150**:1330–1340

20. Austin M. J., Kalampalika F., Cawthorn W. P., Patel B (2023) **Turning the spotlight on bone marrow adipocytes in haematological malignancy and non-malignant conditions** *Br. J. Haematol* **201**:605–619

21. Tratwal J., et al. (2020) **Reporting Guidelines, Review of Methodological Standards, and Challenges Toward Harmonization in Bone Marrow Adiposity Research** *Report of the Methodologies Working Group of the International Bone Marrow Adiposity Society. Front. Endocrinol* **11**

22. Zhang D., et al. (2022) **The microbiota regulates hematopoietic stem cell fate decisions by controlling iron availability in bone marrow** *Cell Stem Cell* **29**:232–247

23. Sjögren K., et al. (2012) **The gut microbiota regulates bone mass in mice** *J. Bone Miner. Res* **27**:1357–1367

24. Quach D., Collins F., Parameswaran N., McCabe L., Britton R. A (2018) **Microbiota Reconstitution Does Not Cause Bone Loss in Germ-Free Mice** *mSphere* **3**:e00545–17

25. Luo Y., et al. (2015) **Microbiota from Obese Mice Regulate Hematopoietic Stem Cell Differentiation by Altering the Bone Niche** *Cell Metab* **22**:886–894

26. Collins S. L., Stine J. G., Bisanz J. E., Okafor C. D., Patterson A. D (2023) **Bile acids and the gut microbiota: metabolic interactions and impacts on disease** *Nat. Rev. Microbiol* **21**:236–247

27. Kuipers F., Bloks V. W., Groen A. K (2014) **Beyond intestinal soap--bile acids in metabolic control** *Nat. Rev. Endocrinol* **10**:488–498

28. Perino A., Demagny H., Velazquez-Villegas L., Schoonjans K (2021) **Molecular physiology of bile acid signaling in health, disease, and aging** *Physiol. Rev* **101**:683–731

29. Perino A., Schoonjans K (2022) **Metabolic Messengers: bile acids** *Nat. Metab* **4**:416–423

30. Kawamata Y., et al. (2003) **A G protein-coupled receptor responsive to bile acids** *J. Biol. Chem* **278**:9435–9440

31. Carino A., et al. (2017) **Gpbar1 agonism promotes a Pgc-1α-dependent browning of white adipose tissue and energy expenditure and reverses diet-induced steatohepatitis in mice** *Sci. Rep* **7**

32. Velazquez-Villegas L. A., et al. (2018) **TGR5 signalling promotes mitochondrial fission and beige remodelling of white adipose tissue** *Nat. Commun* **9**

33. Perino A., et al. (2014) **TGR5 reduces macrophage migration through mTOR-induced C/EBPβ differential translation** *J. Clin. Invest* **124**:5424–5436

34. Eggink H. M., et al. (2018) **Chronic infusion of taurolithocholate into the brain increases fat oxidation in mice** *J. Endocrinol* **236**:85–97

35. Broeders E. P. M., et al. (2015) **The Bile Acid Chenodeoxycholic Acid Increases Human Brown Adipose Tissue Activity** *Cell Metab* **22**:418–426

36. Watanabe M., et al. (2006) **Bile acids induce energy expenditure by promoting intracellular thyroid hormone activation** *Nature* **439**:484–489

37. Persaud A. K., et al. (2021) **Facilitative lysosomal transport of bile acids alleviates ER stress in mouse hematopoietic precursors** *Nat. Commun* **12**

38. Sigurdsson V., et al. (2016) **Bile Acids Protect Expanding Hematopoietic Stem Cells from Unfolded Protein Stress in Fetal Liver** *Cell Stem Cell* **18**:522–532

39. Sigurdsson V., et al. (2020) **Induction of blood-circulating bile acids supports recovery from myelosuppressive chemotherapy** *Blood Adv* **4**:1833–1843

40. Thompson B., et al. (2023) **Secondary bile acids function through the vitamin D receptor in myeloid progenitors to promote myelopoiesis** *Blood Adv. bloodadvances* **2022009618** https://doi.org/10.1182/bloodadvances.2022009618

41. Perino A., et al. (2021) **Central anorexigenic actions of bile acids are mediated by TGR5** *Nat. Metab* **3**:595–603

42. Li Z., et al. (2018) **Dual Targeting of Bile Acid Receptor-1 (TGR5) and Farnesoid X Receptor (FXR) Prevents Estrogen-Dependent Bone Loss in Mice** *J. Bone Miner. Res. jbmr* https://doi.org/10.1002/jbmr.3652

43. Nagano K., et al. (2022) **R-spondin 3 deletion induces Erk phosphorylation to enhance Wnt signaling and promote bone formation in the appendicular skeleton** *eLife* **11**

44. Berendsen A. D., Olsen B. R. (2015) **Bone development** *Bone* **80**:14–18

45. Scheller E. L., et al. (2014) **Use of Osmium Tetroxide Staining with Microcomputerized Tomography to Visualize and Quantify Bone Marrow Adipose Tissue In Vivo** *Methods in Enzymology* :123–139

46. Scheller E. L., et al. (2015) **Region-specific variation in the properties of skeletal adipocytes reveals regulated and constitutive marrow adipose tissues** *Nat. Commun* **6**

47. Tratwal J., et al. (2020) **MarrowQuant Across Aging and Aplasia: A Digital Pathology Workflow for Quantification of Bone Marrow Compartments in Histological Sections** *Front. Endocrinol* **11**

48. Li Z., Hardij J., Bagchi D. P., Scheller E. L., MacDougald O. A (2018) **Development, regulation, metabolism and function of bone marrow adipose tissues** *Bone* **110**:134–140

49. Tencerova M., et al. (2018) **High-Fat Diet-Induced Obesity Promotes Expansion of Bone Marrow Adipose Tissue and Impairs Skeletal Stem Cell Functions in Mice: HFD AFFECTS BM-MSC PROPERTIES AND INSULIN SENSITIVITY IN MICE** *J. Bone Miner. Res* **33**:1154–1165

50. Campos V., Rappaz B., Kuttler F., Turcatti G., Naveiras O (2018) **High-throughput, nonperturbing quantification of lipid droplets with digital holographic microscopy** *J. Lipid Res* **59**:1301–1310

51. Sun H., et al. (2013) **Osteoblast-Targeted suppression of PPARγ increases osteogenesis through activation of mTOR signaling** *Stem Cells* **31**:2183–2192

52. Cock T., et al. (2004) **Enhanced bone formation in lipodystrophic PPARγ hyp/hyp mice relocates haematopoiesis to the spleen** *EMBO Rep* **5**:1007–1012

53. Morowski M., et al. (2013) **Only severe thrombocytopenia results in bleeding and defective thrombus formation in mice** *Blood* **121**:4938–4947

54. Vannini N., et al. (2019) **The NAD-Booster Nicotinamide Riboside Potently Stimulates Hematopoiesis through Increased Mitochondrial Clearance** *Cell Stem Cell* **24**:405–418

55. Inoue K., et al. (2023) **Bone marrow Adipoq-lineage progenitors are a major cellular source of M-CSF that dominates bone marrow macrophage development, osteoclastogenesis, and bone mass** *eLife* **12**

56. Rosen C. J., Horowitz M. C (2023) **Nutrient regulation of bone marrow adipose tissue: skeletal implications of weight loss** *Nat. Rev. Endocrinol* https://doi.org/10.1038/s41574-023-00879-4

57. Devlin M. J (2011) **Why does starvation make bones fat?** *Am. J. Hum. Biol. Off. J. Hum. Biol. Counc* **23**:577–585

58. Devlin M. J., et al. (2010) **Caloric restriction leads to high marrow adiposity and low bone mass in growing mice** *J. Bone Miner. Res* **25**:2078–2088

59. Doucette C. R., et al. (2015) **A High Fat Diet Increases Bone Marrow Adipose Tissue (MAT) But Does Not Alter Trabecular or Cortical Bone Mass in C57BL/6J Mice** *J. Cell. Physiol* **230**:2032–2037

60. Li Z., et al. (2022) **Lipolysis of bone marrow adipocytes is required to fuel bone and the marrow niche during energy deficits** *eLife* **11**

61. Turner R. T., Martin S. A., Iwaniec U. T (2018) **Metabolic Coupling Between Bone Marrow Adipose Tissue and Hematopoiesis** *Curr. Osteoporos. Rep* **16**:95–104

62. Mohty M., et al. (2020) **Prophylactic, preemptive, and curative treatment for sinusoidal obstruction syndrome/veno-occlusive disease in adult patients: a position statement from an international expert group** *Bone Marrow Transplant* **55**:485–495

63. Ueda H., et al. (2022) **Sex-, age-, and organ-dependent improvement of bile acid hydrophobicity by ursodeoxycholic acid treatment: A study using a mouse model with human-like bile acid composition** *PloS One* **17**

64. Heuman D. M (1989) **Quantitative estimation of the hydrophilic-hydrophobic balance of mixed bile salt solutions** *J. Lipid Res* **30**:719–730

65. Shen Y., et al. (2022) **Ursodeoxycholic acid reduces antitumor immunosuppression by inducing CHIP-mediated TGF-β degradation** *Nat. Commun* **13**

66. Zhang H., Xu H., Zhang C., Tang Q., Bi F (2021) **Ursodeoxycholic acid suppresses the malignant progression of colorectal cancer through TGR5-YAP axis** *Cell Death Discov* **7**

67. Ibrahim E., et al. (2018) **Bile acids and their respective conjugates elicit different responses in neonatal cardiomyocytes: role of Gi protein, muscarinic receptors and TGR5** *Sci. Rep* **8**

68. Sepe V., et al. (2014) **Modification on ursodeoxycholic acid (UDCA) scaffold. discovery of bile acid derivatives as selective agonists of cell-surface G-protein coupled bile acid receptor 1 (GP-BAR1)** *J. Med. Chem* **57**:7687–7701

69. Sato H., et al. (2008) **Novel potent and selective bile acid derivatives as TGR5 agonists: biological screening, structure-activity relationships, and molecular modeling studies** *J. Med. Chem* **51**:1831–1841

70. Li Y.-X., et al. (2017) **Investigation of triamterene as an inhibitor of the TGR5 receptor: identification in cells and animals** *Drug Des. Devel. Ther.* **11**:1127–1134

71. Masyuk T. V., et al. (2017) **TGR5 contributes to hepatic cystogenesis in rodents with polycystic liver diseases through cyclic adenosine monophosphate/Gαs signaling** *Hepatology* **66**:1197–1218

72. Thirouard L., et al. (2022) **Identification of a Crosstalk among TGR5, GLIS2, and TP53 Signaling Pathways in the Control of Undifferentiated Germ Cell Homeostasis and Chemoresistance** *Adv. Sci* **9**

73. Thomas C., et al. (2009) **TGR5-Mediated Bile Acid Sensing Controls Glucose Homeostasis** *Cell Metab* **10**:167–177

74. Bouxsein M. L., et al. (2010) **Guidelines for assessment of bone microstructure in rodents using micro-computed tomography** *J. Bone Miner. Res* **25**:1468–1486

75. Maridas D. E., Rendina-Ruedy E., Le P. T., Rosen C. J. (2018) **Isolation, Culture, and Differentiation of Bone Marrow Stromal Cells and Osteoclast Progenitors from Mice** *J. Vis. Exp. JoVE* **56750** https://doi.org/10.3791/56750

Article and author information

Alejandro Alonso-Calleja

Laboratory of Regenerative Hematopoiesis, Department of Biomedical Sciences, University of Lausanne, Switzerland, Laboratory of Metabolic Signaling, Institute of Bioengineering, Ecole Polytechnique Fédérale de Lausanne, Lausanne, Switzerland
ORCID iD: 0000-0003-0864-5375

Alessia Perino

Laboratory of Metabolic Signaling, Institute of Bioengineering, Ecole Polytechnique Fédérale de Lausanne, Lausanne, Switzerland

Frédérica Schyrr

Laboratory of Regenerative Hematopoiesis, Department of Biomedical Sciences, University of Lausanne, Switzerland

Silvia Ferreira Lopes
Laboratory of Regenerative Hematopoiesis, Department of Biomedical Sciences, University of Lausanne, Switzerland

Vasiliki Delitsikou
Laboratory of Metabolic Signaling, Institute of Bioengineering, Ecole Polytechnique Fédérale de Lausanne, Lausanne, Switzerland

Antoine Jalil
Laboratory of Metabolic Signaling, Institute of Bioengineering, Ecole Polytechnique Fédérale de Lausanne, Lausanne, Switzerland

Ulrike Kettenberger
Laboratory of Biomechanical Orthopedics, Ecole Polytechnique Fédérale de Lausanne, Lausanne, Switzerland

Dominique P. Pioletti
Laboratory of Biomechanical Orthopedics, Ecole Polytechnique Fédérale de Lausanne, Lausanne, Switzerland
ORCID iD: 0000-0001-5535-5296

Kristina Schoonjans
Laboratory of Metabolic Signaling, Institute of Bioengineering, Ecole Polytechnique Fédérale de Lausanne, Lausanne, Switzerland
For correspondence: olaia.naveiras@unil.ch
ORCID iD: 0000-0003-1247-4265

Olaia Naveiras
Laboratory of Regenerative Hematopoiesis, Department of Biomedical Sciences, University of Lausanne, Switzerland, Hematology Service, Departments of Oncology and Laboratory Medicine, Lausanne University Hospital (CHUV) and University of Lausanne (UNIL), Lausanne, Switzerland
For correspondence: olaia.naveiras@unil.ch
ORCID iD: 0000-0003-3434-0022

Copyright

Editors

Reviewing Editor
Owen Tamplin
University of Wisconsin-Madison, Madison, United States of America

Senior Editor
Sofia Araújo
University of Barcelona, Barcelona, Spain

Reviewer #1 (Public Review):

Summary:
Alonso-Calleja and colleagues explore the role of TGR5 in adult hematopoiesis at both steady state and post-transplantation. The authors utilize two different mouse models including a TGR5-GFP reporter mouse to analyze the expression of TGR5 in various hematopoietic cell subsets. Using germline Tgr5-/- mice it's reported that loss of Tgr5 has no significant impact on steady-state hematopoiesis, with a small decrease in trabecular bone fraction, associated with a reduction in proximal tibia adipose tissue, and an increase in marrow phenotypic adipocytic precursors. The authors further explored the role of stroma TGR5 expression in the hematopoietic recovery upon bone marrow transplantation of wild-type cells, although the studies supporting this claim are weak. Overall, while most of the hematopoietic phenotypes have negative results or small effects, the role of TGR5 in adipose tissue regulation is interesting to the field.

Strengths:
• This is the first time the role of TGR5 has been examined in the bone marrow.
• This paper supports further exploration of the role of bile acids in bone marrow transplantation and possible therapeutic strategies.

Weaknesses:
• The authors fail to describe whether niche stroma cells or adipocyte progenitor cells (APCs) express TGR5.
• Although the authors note a significant reduction in bone marrow adipose tissue in Tgr5-/- mice, they do not address whether this is white or brown adipose tissue especially since BA-TGR5 signaling has been shown to play a role in beiging.
• In Figure 1, the authors explore different progenitor subsets but stop short of describing whether TGR5 is expressed in hematopoietic stem cells (HSCs).
• Are there more CD45+ cells in the BM because hematopoietic cells are proliferating more due to a direct effect of the loss of Tgr5 or is it because there is just more space due to less trabecular bone?
• In Figure 4 no absolute cell counts are provided to support the increase in immunophenotypic APCs (CD45-Ter119-CD31-Sca1+CD24-) in the stroma of Tgr5-/- mice. Accordingly, the absolute number of total stromal cells and other stroma niche cells such as MSCs, ECs are missing.
• There are issues with the reciprocal transplantation design in Fig 4. Why did the authors choose such a low dose (250 000) of BM cells to transplant? If the effect is true and relevant, the early recovery would be observed independently of the setup and a more robust engraftment dataset would be observed without having lethality post-transplant. On the same note, it's surprising that the authors report ~70% lethality post-transplant from wild-type control mice (Fig 4E), according to the literature 200 000 BM cells should ensure the survival of the recipient post-TBI. Overall, the results even in such a stringent setup still show minimal differences and the study lacks further in-depth analyses to support the main claim.
• Mechanistically, how does the loss of Tgr5 impact hematopoietic regeneration following sublethal irradiation?
• Only male mice were used throughout this study. It would be beneficial to know whether female mice show similar results.

https://doi.org/10.7554/eLife.93124.1.sa1

Reviewer #2 (Public Review):

Summary: In this manuscript, the authors examined the role of the bile acid receptor TGR5 in the bone marrow under steady-state and stress hematopoiesis. They initially showed the

expression of TGR5 in hematopoietic compartments and that loss of TGR5 doesn't impair steady-state hematopoiesis. They further demonstrated that TGR5 knockout significantly decreases BMAT, increases the APC population, and accelerates the recovery upon bone marrow transplantation.

Strengths: The manuscript is well-structured and well-written.

Weaknesses: The mechanism is not clear, and additional studies need to be performed to support the authors' conclusion.

https://doi.org/10.7554/eLife.93124.1.sa0